Hindawi
International Journal of Energy Research
Volume 2023, Article ID 1287144, 9 pages
https://doi.org/10.1155/2023/1287144

WILEY | Hindawi

Research Article

Generation of Stable Photovoltage in Nonstoichiometric $CuBi_2O_4$ Thin-Film Photocathodes

Jaeyong Woo,[1,2] Jongmin Lee,[1,3] Jinsol Jun,[1] Seungkyu Kim,[1] Yoonsung Jung,[1] Inhyeok Oh,[1] and Sanghan Lee[1]

[1]*School of Materials Science and Engineering, Gwangju Institute of Science and Technology, Gwangju 61005, Republic of Korea*
[2]*Package Sejong Manufacturing Technology Group, Package Solution Business Unit, Samsung Electro-Mechanics Co., Ltd, Sejong 30067, Republic of Korea*
[3]*Department of Materials Science & Engineering and Materials Research Laboratory, University of Illinois at Urbana-Champaign, Urbana, Illinois 61801, USA*

Correspondence should be addressed to Sanghan Lee; sanghan@gist.ac.kr

Received 11 October 2022; Revised 13 December 2022; Accepted 20 January 2023; Published 16 February 2023

Academic Editor: Subhash Singh

We investigated the effects of stoichiometry on photovoltages and photocurrents in $CuBi_2O_4$ thin-film photocathodes grown by pulsed laser deposition under different oxygen partial pressures to manipulate their stoichiometry. While the X-ray diffraction patterns show crystalline phases in the $CuBi_2O_4$ thin films, it is found that the Cu/Bi ratio of the $CuBi_2O_4$ thin films varied from ~0.3 to ~0.5 which are analyzed by X-ray photoelectron spectroscopy and energy-dispersive X-ray spectroscopy. The slightly off-stoichiometric $CuBi_2O_4$ thin-film photocathode with a Cu/Bi ratio of ~0.44 shows the highest photocurrent density in the $CuBi_2O_4$ thin films. More interestingly, the off-stoichiometric $CuBi_2O_4$ thin-film photocathode with a Cu/Bi ratio of ~0.44 exhibited a stable open-circuit voltage difference of ~0.2 V_{RHE} without severe degradation over time. On the other hand, the photovoltage of the stoichiometric $CuBi_2O_4$ thin-film photocathode with a Cu/Bi ratio of ~0.5 gradually decreased as a function of time. Our results suggest that stoichiometry manipulation can be one of the promising strategies to achieve long-term stable Cu-based oxide photocathodes with the maintenance of a stable photovoltage.

1. Introduction

Chemical stoichiometry is key to determining physical properties of materials and functionality of various electronic and energy devices [1–4]. Tuning the stoichiometry of oxide thin-film photoelectrodes used in photoelectrochemical (PEC) water splitting changes not only their charge-transport properties by employing phase transitions but also their cation oxidation states, which affect the oxidation or reduction of water on a photoelectrode surface [5–8]. Furthermore, the impact of surface stoichiometry has been increasing with the development of complex metal oxide photoelectrodes toward high photocurrent density and long-term stability [9–11]. For example, the surface cation ratio of $BiVO_4$ thin-film photoanodes has been investigated systematically to understand fundamental photocurrent generation in terms of the oxygen evolution reaction [9]. Interest into the development of stable photoelectrodes has been increasing gradually; however, the effect of stoichiometry on oxide photocathodes has been investigated to a relatively less extent due to scarce photocathode candidates caused by their poor stability, such as photocorrosion under aqueous environments in well-known p-type semiconductor oxides including Cu-based binary oxides [12, 13]. Although Cu-based oxide photocathodes can be catalytically stabilized depending on their stoichiometry, to our best knowledge, the fundamental relationship between the stoichiometry and photoelectrochemical properties of Cu-based oxide photocathodes has been rarely investigated. Thus, it is imperative to examine the relationship between

stoichiometry and PEC properties to develop robust oxide semiconductor photocathodes.

Cu-based oxide photocathodes are well known to exhibit advantages of earth-abundant Cu and narrow band gaps of ~2 eV, which enable the efficient absorption of light energy [14]. Among the interesting Cu-based oxide photocathode candidates, ternary oxide $CuBi_2O_4$ (CBO) demonstrates promise due to its narrow band gap of ~1.8 eV and considerable photovoltage originating from a high onset potential of greater than 1 V_{RHE} [15, 16]. Recently, CBO photocathodes were reported to exhibit an excellent PEC performance with a high photocurrent density of approximately -3.5 mA/cm^2 at a potential of 0.4 V_{RHE} and long-term stability of greater than 8 h at a potential of 0.4 V_{RHE} [17, 18]. CBO is expected to be used as an oxide photocathode for efficient green hydrogen production as well as reduction of CO_2 to valuable chemicals [19, 20]; however, owing to its poor surface catalytic behavior, it is not durable as a photocathode for use in practical PEC water splitting. These limitations motivated us to shift our investigation from performance improvement to the fundamental investigation of CBO photocathodes. For example, the fundamental studies require a well-defined thin-film structure and pure crystalline phases such as single-crystalline and polycrystalline states of the CBO thin-film photocathodes [18, 21]. And the Cu/Bi stoichiometry ratio could be also controlled by pulsed laser deposition (PLD) and rapid thermal processing for the synthesis of the pure CBO phase [22, 23]. In addition, Oropeza et al. reported that surface states of the substoichiometric $CuBi_2O_{4-x}$ layer affect surface band bending, which improves charge-carrier transport properties [24]. These results reveal that stoichiometry manipulation affects PEC properties of the CBO photocathodes. Accordingly, it is imperative to understand the relationship between stoichiometry and PEC properties to overcome catalytic degradation such as photocorrosion, originating from the sluggish surface-exchange kinetics in CBO photocathodes [25].

Measurement of open-circuit potential (OCP), involving the measurement of photovoltage under chopping light illumination, is one of the easiest technical methods to practically investigate light-induced electrochemical reactions involving the generation of photogenerated charge carriers and their recombination in PEC cells [26]. From OCP measurement, the flat band potential of the semiconductor photoelectrode can be estimated via the measurement of the band bending formed at the photoelectrode surface with the electrolyte [27]. To examine the photostability and surface states of various photoelectrodes as well as enhance open-circuit voltage (V_{oc}), OCP measurements were conducted to understand thermodynamic stability, including photocorrosion reactions [28]. In particular, OCP differences under various bubbling gases and morphologies were measured to identify the surface states for achieving durable CBO photocathodes [29]. However, some undesirable geometric factors such as uneven morphology and exposed bottom electrode hinder reliable comparison in terms of the fundamental investigation of CBO photocathodes. Hence, a well-defined geometric structure is mandatory to overcome the photocorrosion of CBO photocathodes. Moreover, the relationship between stoichiometry and OCP changes as a function of time on the CBO photocathode has not been investigated systematically.

In this study, we fabricated polycrystalline CBO thin films grown by PLD under controlled oxygen partial pressures to investigate the effects of stoichiometry on photocurrent/photovoltage of CBO thin films. Notably, PLD is well known to grow well-defined geometric thin films under systematic changes in various growth parameters (e.g., temperature [30], oxygen partial pressure [31], and laser energy [32]). In particular, the control of the oxygen partial pressure in PLD induces a systematic change in the cation/oxygen stoichiometry of complex oxide thin films [33]. Energy-dispersive X-ray spectroscopy (EDX) and X-ray photoelectron spectroscopy (XPS) confirm that the cation ratio (Cu/Bi) of CBO thin films is clearly dependent on the oxygen partial pressure (60, 200, and 600 mTorr). With the increase in the oxygen partial pressure, the cation ratio of Cu/Bi is similar to that of stoichiometric CBO. Notably, a high photocurrent density and stable photovoltage generation are achieved in a slightly off-stoichiometric CBO thin film, while an identical optical band gap of ~1.94 eV is observed for CBO thin films. The photocurrent density trend of the CBO thin-film photocathode will be discussed in conjunction with their chopped OCP measurements and stoichiometry change.

2. Experimental Section

2.1. Fabrication of a $CuBi_2O_4$ Ceramic Target. High-purity oxide precursors of pure Bi_2O_3 (Kojundo Chemical Lab Co., Ltd., Japan; purity: 99.99%, 5–10 μm) and CuO (Kojundo Chemical Lab Co., Japan; purity: 99.9%, 1 μm) were used as raw materials. Bi_2O_3 and CuO powder were mixed in a molar ratio of 1 : 1 by wet milling for 100 min in a stainless-steel jar using a planetary ball mill (Fritsch, Pulverisette 5 Planetary Mill) at 350 rpm. ZrO_2 ceramic balls (diameter: 5 mm) and ethyl alcohol were used as the milling medium and solvent, respectively. After mixing, the powders were dried at 120°C for 24 h in an oven, and the dried powders were subsequently calcined at 600°C for 20 h in a box furnace to synthesize the CBO phase.

Next, the calcined CBO powders were crushed in an agate mortar with a pestle. The crushed powders were uniaxially pressed into a cylindrical target under ~7 MPa. After the green target was sintered at 720°C for 24 h, the sintered CBO target with a diameter of ~20 mm and a thickness of ~5 mm was obtained. The relative mass density of this target was confirmed to be ~94% by the Archimedes method using deionized water.

2.2. Preparation of $CuBi_2O_4$ Thin-Film Photocathodes. Polycrystalline CBO thin films were grown on the fluorine-doped tin-oxide glass substrate (FTO glass, Pilkington, TEC 15) by PLD equipped with a KrF (248 nm) excimer laser (Coherent COMPexPro 205F, λ = 248 nm). To deposit CBO thin films with a controlled cation ratio, oxygen partial pressures were controlled at 60, 200, and 600 mTorr (Figure 1(a)). The base pressure, laser energy density, and repetition rate were

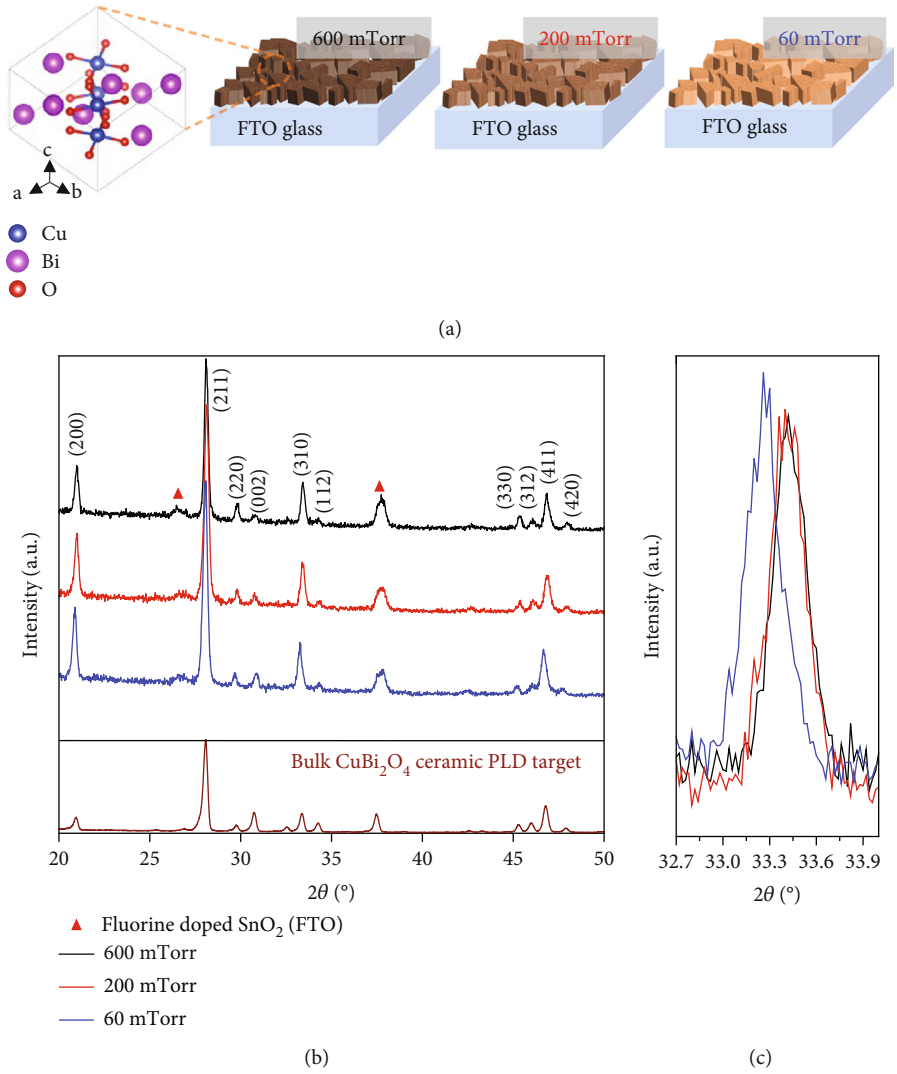

FIGURE 1: (a) Schematic of the $CuBi_2O_4$ crystal structure and its thin films grown by pulsed laser deposition under controlled oxygen partial pressures. (b) X-ray diffraction patterns of the films grown on FTO substrate and PLD target. (c) Enlarged Braggs peak (310) region.

3.0×10^{-6} Torr, 2.0 J/cm^2, and 10 Hz, respectively. The CBO thin-film thickness was 800 nm. Hereafter, CBO thin films grown at 60, 200, and 600 mTorr will be referred to as CBO–60, CBO–200, and CBO–600, respectively.

2.3. Photoelectrochemical Measurements. PEC measurements were conducted under an illumination source (AM 1.5G, 100 mW/cm^2) using a 150-W xenon lamp (Model 10500, ABET Technology) with a three-electrode system, including the photocathodes (CBO-60, CBO-200, and CBO-600) as the working electrode, graphite as the counter electrode, and [Ag/AgCl (saturated KCl)] as the reference electrode. The potential versus a reversible hydrogen electrode (V_{RHE}) was calculated using the following equation:

$V_{RHE} = V_0\,\text{Ag/AgCl (saturated KCl)} + \text{VAg/ AgCl} + 0.059 \times \text{pH}$, where V_0 Ag/AgCl (saturated KCl) = 0.197 V at 25°C. The electrolyte of the potassium phosphate buffer solution (0.1 M, pH 8.55) was prepared by mixing 0.1 M potassium phosphate monobasic (Sigma Aldrich, ≥98.0%) and 0.1 M potassium phosphate dibasic (Sigma Aldrich, ≥98.0%). PEC measurements were performed using two electrolytes: potassium phosphate buffer solution (pH ~8.55) with and without H_2O_2 as the hole scavenger (pH ~8.55). We carried out PEC measurements to estimate photovoltages of $CuBi_2O_4$ thin films using chronopotentiometry measurement mode. Note that the open-circuit voltage is obtained by potential difference when photoelectrode is exposed to light illumination from dark mode. Dark/light chopping is automatically controlled per 10 s through Thorlabs APT User software in this work (Thorlabs MFF101/M).

3. Results and Discussion

Figure 1(b) shows powder X-ray diffraction (XRD) patterns of polycrystalline CBO thin films grown on FTO glass substrates as a function of oxygen partial pressures (600 (top), 200 (middle), and 60 (bottom) mTorr). Even though the oxygen partial pressure was varied from 60 to 600 mTorr for as-grown CBO thin films, the main Bragg reflections corresponding to CBO are observed, including strong (211)

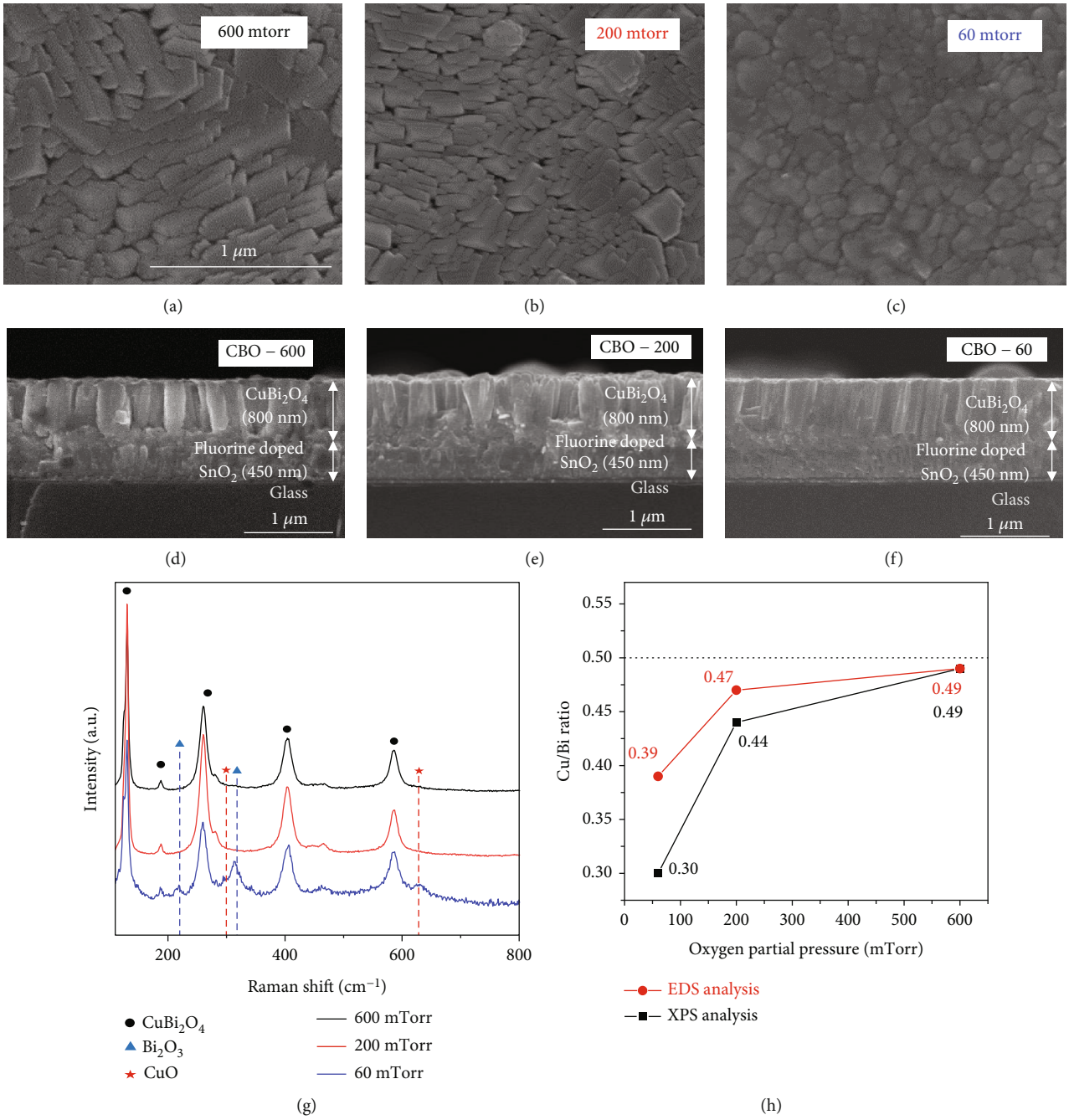

Figure 2: Topographic surface and cross-sectional SEM images of $CuBi_2O_4$ thin films under controlled oxygen partial pressures of (a, d) 600, (b, e) 200, and (c, f) 60 mTorr. (g) Raman spectra and (h) estimated cation ratio of the $CuBi_2O_4$ thin films (thickness ~800 nm) depending on their oxygen partial pressures. Note that the dashed line indicates the cation ratio (Cu/Bi = 1/2) of the stoichiometric $CuBi_2O_4$.

diffraction peaks at $2\theta \sim 28^\circ$. In addition, the CBO peaks are well indexed to those of the bulk CBO ceramic target. Notably, the thickness of the CBO thin films is maintained at 800 nm to remove effects of thickness on the structural and PEC properties between the CBO thin films (Figures 2(d)–2(f)). Meanwhile, in our previous studies, poly- and single-crystalline CBO thin films are grown by PLD under an oxygen partial pressure of 300 mTorr [18, 21]. Considering the low oxygen background-gas pressure environments of the CBO thin film under 60 mTorr compared to our previous growth condition of CBO thin films, the cation stoichiometry of the CBO thin film grown at a pressure of 60 mTorr is expected to be distinct to those of CBO thin films grown under oxygen partial pressures of 200 and 600 mTorr. While the substrate peak positions between samples are overlapped, the (310) peak of CBO-60 is shifted to as low as $2\theta \sim 0.1^\circ$ compared with those of CBO-200 and CBO-600, as shown in Figure 1(c), corresponding to a d-spacing difference of ~0.1 Å in the CBO lattice structure. This result indicates that the control of oxygen

partial pressure can induce lattice parameter modification, originating from changes in the cation/oxygen stoichiometry of the CBO thin films. Notably, the incorporation of oxygen vacancies could induce the expansion of the lattice structure in oxide compounds [34].

To understand the dependence of microstructures on the oxygen partial pressure, topographic surface measurements of CBO-60, CBO-200, and CBO-600 by scanning electron microscopy (SEM) and atomic force microscopy (AFM) were conducted (Figures 2(a)–2(c)) (for AFM images, check supplementary Figure S1). The surface morphologies of CBO-60, CBO-200, and CBO-600 revealed smooth, dense, and crystalline grains, which are features of CBO thin films grown by PLD [21]. Meanwhile, the surface roughness (root mean square roughness (R_q) ~8.6 nm) of CBO-60 with circular grains is slightly less than those of CBO-600 (R_q ~15.3 nm) and CBO-200 (R_q ~12.5 nm).

To determine the discrepancy in changes in the lattice expansion and surface morphologies of CBO-60, CBO-200, and CBO-600, Raman spectra of CBO thin films (CBO-60, CBO-200, and CBO-600) were measured as shown in Figure 2(d)]. The Raman spectra of CBO-200 and CBO-600 are well matched with those of previously reported pure CBO phases [35], whereas the Raman spectrum of CBO-60 exhibits peaks corresponding to those of CuO and Bi_2O_3, indicating that CBO-60 is formed by CBO composites with secondary phases such as CuO and Bi_2O_3. These results suggest that a low oxygen partial pressure leads to the formation of secondary phases beyond the nonstoichiometry of the CBO thin films. That is, the oxygen deficiency induces cation modulation via decomposition in the CBO thin films. Furthermore, the control of the cation ratio of Cu/Bi modifies the morphologies and phase formation [36]. Thus, the optimum oxygen partial pressure of 200–600 mTorr is selected for the synthesis of pure CBO thin films without the formation of secondary phases based on Raman spectra and surface morphology analyses. In addition, EDX and XPS compositional analyses of CBO thin films were conducted to estimate the cation ratio between copper (Cu) and bismuth (Bi) in the CBO thin films (Figure 2(e)) (for EDX and XPS survey scans, check supplementary Figure S2). Notably, the vertical axis of the Cu/Bi ratio corresponds to the atomic percentage ratio of the measured cations; hence, a Cu/Bi ratio of ~0.5 indicates stoichiometric CBO. If the horizontal axis of the Cu/Bi ratio is less than 0.5 (dotted horizontal black line in Figure 2(e)), the Cu-deficient CBO, Bi-rich CBO, and Bi_2O_3 secondary phases would be formed in the CBO thin films. With the increase in the oxygen partial pressure from 60 to 600 mTorr, the Cu/Bi ratio is closer to 0.5, as confirmed by EDS and XPS analyses. In particular, the Cu/Bi ratio (0.39 (EDS) and 0.30 (XPS)) of CBO-60 is more deviated from 0.5 than those of CBO-200 and CBO-600. Considering that Raman spectra reveal secondary phases such as Bi_2O_3 in CBO-60, a low Cu/Bi ratio of less than 0.4 would promote the decomposition of CBO, with secondary phases such as CuO and Bi_2O_3 in CBO-60. By contrast, Cu/Bi ratios of 0.4–0.5 are observed in CBO thin films, exhibiting pure CBO phases with no formation of secondary phases, under oxygen partial pressures of 200 and 600 mTorr.

To investigate the dependence of the optical difference of CBO thin films on the oxygen partial pressure, optical absorbances of CBO-60, CBO-200, and CBO-600 were measured using an ultraviolet-visible spectrometer, as shown in the inset of Figure 3(a). The absorbances of CBO-60, CBO-200, and CBO-600 reveal comparable spectra across wavelength ranges as CBO thin films are formed by dominant CBO phases. Meanwhile, the absorbance of CBO-60 is slightly less than those of CBO-200 and CBO-600 in the wavelength range of 400–1000 nm. This result might be related to the formation of CBO-Bi_2O_3 composites in CBO-60. Next, Tauc plots of $(ah\nu)1/r$ also were recorded to estimate optical band gaps of CBO-60, CBO-200, and CBO-600. Their band gaps were estimated to be ~1.94 eV, which is similar to previously reported values [16, 18]. This result indicates that the CBO phases in the CBO thin films are dominant regardless of the CBO-Bi_2O_3 compositions of CBO-60, CBO-200, and CBO-600.

The photocurrent densities of CBO thin-film photocathodes (CBO-60, CBO-200, and CBO-600) were investigated under dark and light illumination, as shown in Figure 3(b). Interestingly, CBO-200 exhibits the highest photocurrent density (-0.33 mA cm^{-2}) at a potential of 0.4 V_{RHE}. Meanwhile, the photocurrent densities of CBO-600 and CBO-60 are -0.13 and -0.15 mA cm^{-2}, respectively. Considering that CBO-60 is a CBO composite with Bi_2O_3, it is expected to exhibit a poor photocurrent density as the light absorbance of Bi_2O_3 is low owing to its wide band gap of ~3 eV [37, 38]. The other notable finding is that the performance of CBO-600 is less than that of CBO-200 in the applied potential range from 0.4 to 1.2 V_{RHE} although the compositional ratio of Cu and Bi approaches 0.5 in CBO-600. Furthermore, at a potential of less 0.4 V_{RHE}, the dark current density of CBO-600 increases sharply in comparison to those of CBO-60 and CBO-200, as shown in the inset of Figure 3(b). To further compare the dependence of the photocurrent stability of CBO-200 and CBO-600 on the oxygen partial pressure, chopped chronoamperometry measurements of CBO-200 and CBO-600 also were performed (Figure 3(c)). The photocurrent density of CBO-200 is greater than that of CBO-600 over time. In particular, the relaxation time at which photocurrent relaxation occurs during the initial ~3 min after switching light illumination was compared to evaluate the photostability of CBO photocathodes. Notably, the relaxation time was defined as 40% of the maximum photocurrent density with spike. The relaxation time of CBO-200 (at ~2.2 min) is considerably faster than that (>3 min) of CBO-600. This result indicates that the overpotential is reduced for driving the hydrogen evolution reaction on a semiconductor photoelectrode and the electrolyte interface in CBO-200, as shown in the inset of Figure 3(c).

To determine discrepancies in the photocurrent relaxation behaviors of CBO-60 and CBO-600, chronopotentiometry was conducted while maintaining zero current for OCV measurements of the 0.1 M KPi solution electrolyte with and without H_2O_2 as the scavenger under dark illumination, as shown in Figures 4(a)–4(f). Notably, OCV measurements reveal a potential difference in terms of the

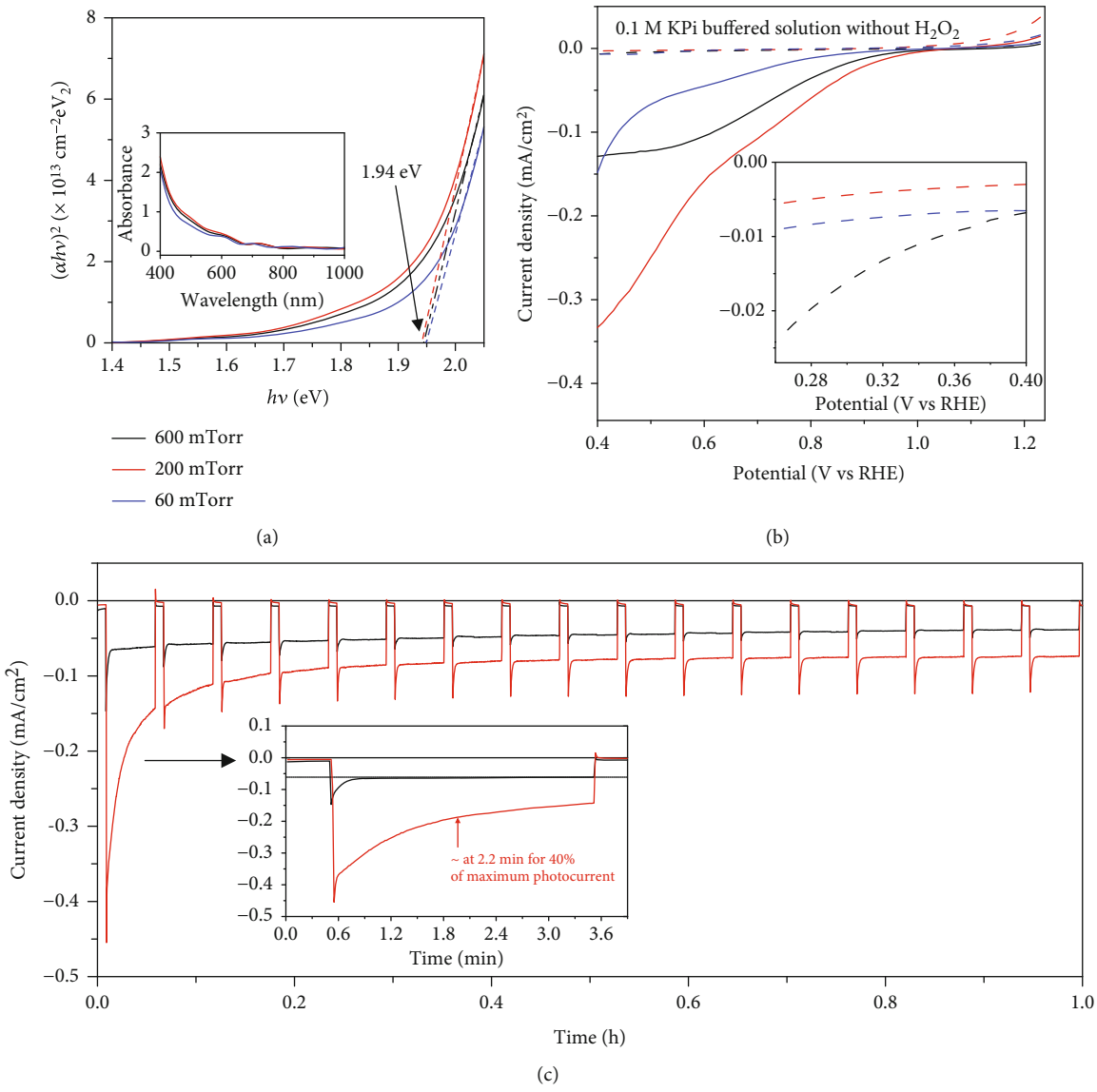

FIGURE 3: (a) Tauc plots obtained from UV-Vis absorbance spectra (inset) and (b) linear sweep voltammetry scans of $CuBi_2O_4$ (thickness ~800 nm) thin-film photocathodes. Inset: Enlarged dark current regions from 0.3 to 0.5 V_{RHE}. Dashed lines and solid lines represent dark-current density and photocurrent density, respectively. (c) Chopped chronoamperometry measurements of $CuBi_2O_4$ thin-film photocathodes at a potential of 0.3 V_{RHE}. These measurements were performed in a 0.1 M KPi buffered solution as the electrolyte without H_2O_2 scavengers.

electrochemical surface reaction at the photoelectrodes, such as charge transfer and surface charge traps [26]. Figures 4(a)–4(c) show the light-chopped OCV results for the electrolyte without H_2O_2 as the scavenger for CBO-60, CBO-200, and CBO-600, respectively. The chopped OCV curves of Cu/Bi ratio-controlled CBO thin-film photoelectrodes (CBO-60, CBO-200, and CBO-600) were relaxed during light on and off. At 10 s, the OCV is ~0.2 V_{RHE} when the light turned on for all samples, which is defined as the photovoltage. Note that the our OCV of ~0.2 V_{RHE} is comparable to that of recent CBO photocathodes [15, 16, 24] (check supplementary Table S1). In particular, CBO-600 exhibits sluggish relaxation compared to the sharp relaxation of CBO-60 and CBO-200 between 10 and 20 s. The OCV potential differences (0.147 V_{RHE} $(t_1 - t_0)$, 0.184 V_{RHE} $(t_2 - t_0)$, and 0.198 V_{RHE} $(t_3 - t_0)$) of CBO-600 gradually increase, indicating that the photogenerated carriers in CBO-600 remain at the bulk/surface regions. Considering that OCV potential differences increase over time in CBO-600, the photogenerated carriers are assumed to be trapped at the photoelectrode surface of CBO-600. By contrast, those of CBO-60 and CBO-200 exhibit relatively stable photovoltage relaxation behaviors even with repeated light chopping. Furthermore, the surface-trapped photogenerated charges were confirmed from light-chopped OCV measurements using the electrolyte with H_2O_2 for all CBO thin films. As expected, a significant difference in the OCV potentials of all samples over time is not observed, as shown in Figures 4(d)–4(f). This result indicates that the photogenerated carriers suffer

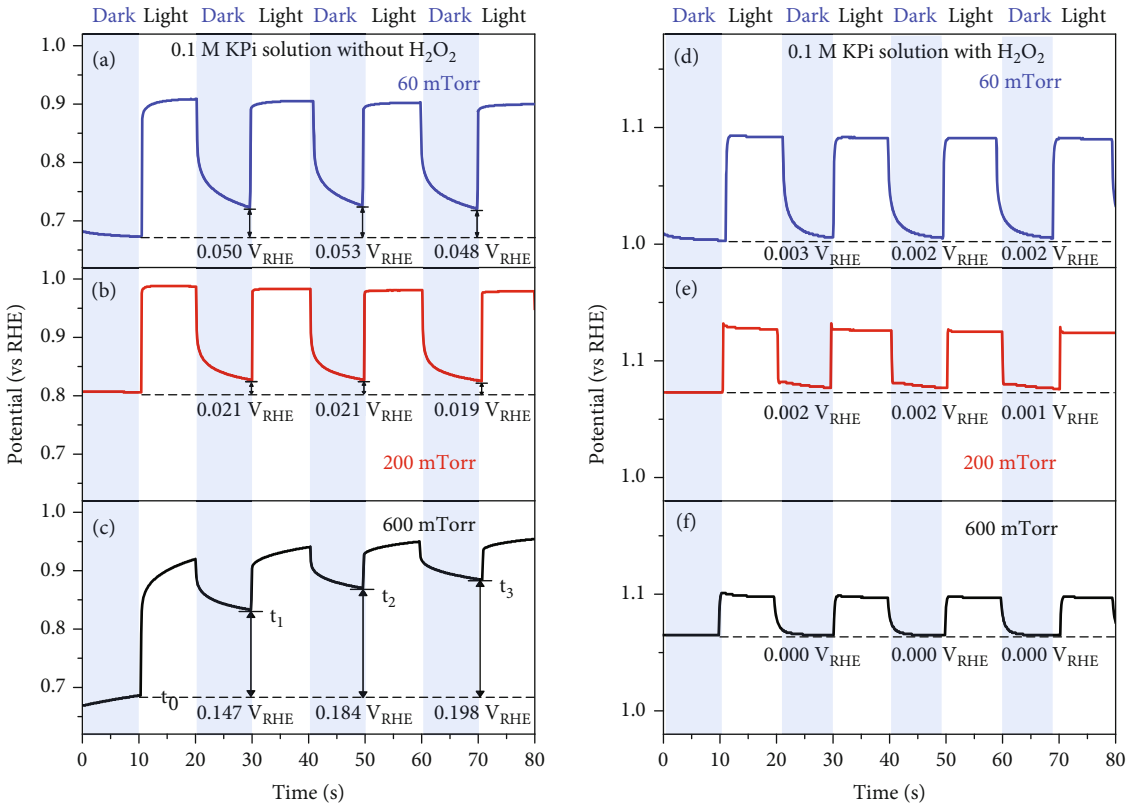

FIGURE 4: Chopped open-circuit potential measurements for $CuBi_2O_4$ thin-film photocathodes in the electrolytes of 0.1 M KPi buffered solution (pH ~8.55) with and without H_2O_2 as the electron scavenger. Notably, the time (t_0, t_1, t_2, and t_3) indicates measured potentials under dark-illumination conditions after 10 s to achieve surface equilibrium.

from sluggish surface kinetics between the electrolyte without H_2O_2 and all CBO thin films. In particular, for CBO-600, the largest OCV difference (0.147–0.198 V_{RHE}) without the scavenger indicates poor surface-exchange behaviors, leading to increased dark current and poor stability caused by self-reduction or recombination in CBO thin films. In addition, the occupancy of Cu oxidation states at a Cu $2p_{3/2}$ binding energy of ~934.1 eV in as-grown CBO-60, CBO-200, and CBO-600 was analyzed (check supplementary Figure S3). The higher the increase in the oxygen partial pressure in PLD, the smaller Cu^{2+} ratio corresponds to ~84%, 66%, and 56% occupancy sites of the surface Cu species for CBO-60, CBO-200, and CBO-600, respectively.

In conjunction with Cu/Bi ratio analyses in Figure 2(h), this result suggests that the slightly Cu-deficient CBO thin films might be beneficial for enhancing the Cu^{2+} concentration, corresponding to an ideal charge valence of Cu^{2+} in the pure CBO phase. In this regard, the preservation of the Cu^{2+} concentration is important to achieve the long-term stability in the CBO thin-film photocathodes. In fact, it was reported that the Cu reduced species (Cu^{1+} or Cu^0) occur upon stability measurements in the single-crystal CBO thin films [21]. The OCV could be increased due to downward band bending by reduced surface state of Cu in the CBO photocathodes [24]. These results imply that the photocorrosion might accompany the reduction of Cu^{2+} and photovoltage increase over time. And Cu deficiency probably shifts Fermi level toward nontrapping of photoelectrons in the Cu 3*d* of the CBO thin film. Although the CuO secondary phases were not observed in our CBO thin films, it would enhance the photovoltage via type-II heterojunction between CuO/CBO even if Cu^{2+} is obtained via CuO segregation in the CBO thin film [39]. Notably, Cu^+ and Cu originate from the reduced species, including Cu_2O secondary phases [24].

4. Conclusion

In summary, CBO thin films (thickness of 800 nm) were fabricated by PLD under the control of oxygen partial pressures (60, 200, and 600 mTorr). Their structural, compositional, optical, and photoelectrochemical properties were analyzed systematically in this work. Oxygen partial pressure-controlled CBO thin films showed the Cu/Bi ratios of 0.3, 0.44, and 0.49 (analyzed by XPS measurements) for CBO-60, CBO-200, and CBO-600, respectively. Additionally, CBO-60 exhibited an off-stoichiometric CBO phase and a secondary phase such as Bi_2O_3 (analyzed by Raman spectroscopy), while CBO-200 and CBO-600 exhibited pure CBO phases only. In particular, the slightly off-stoichiometric CBO-200 exhibited the highest photocurrent density (-0.33 mA/cm^2 at a potential of 0.4 V_{RHE}) and relatively stable photocurrent density as a function of time in the CBO thin films. It was found that the photovoltage difference of CBO-600 gradually increased from 0.147 to

0.198 V_{RHE} over time under the repeated switching of light. By contrast, CBO-200 exhibited relatively stable photovoltages with small OCV differences around 0.20 V_{RHE} over time. Our OCV potential analyses suggest that the slightly Cu-deficient CBO phases could exhibit stable photovoltage generation via fast surface kinetics between the electrolyte and the surface of CBO thin-film photocathodes. Our studies would be beneficial to optimize the growth of CBO thin films for the subsequent enhancement of their photocurrent density and the photoelectrochemical properties of CBO photocathodes via the control of the modest cation off-stoichiometry between Cu and Bi in CBO thin films.

Data Availability

Data will be made available on request.

Conflicts of Interest

The authors declare that there are no conflicts of interest regarding the publication of this paper.

Authors' Contributions

J. Woo, J. Lee, and J. Jun contributed equally to this work.

Acknowledgments

This study was supported by the National Research Foundation of Korea (NRF) grant funded by the Korea Government (MSIT) (No. 2020R1A2C1005590), as well as by the program of Future Hydrogen Original Technology Development (2021M3I3A1084747) through the NRF, funded by the Korea government (Ministry of Science and ICT (MSIT)). This study was also supported by the Basic Science Research Program through the NRF funded by the Korea government (Ministry of Education) (2020R1A6A3A01099847).

Supplementary Materials

Additional supporting information (topographic AFM images, EDS, wide-scan and narrow scan XPS spectra, and summary of stability and open-circuit voltages of $CuBi_2O_4$ photocathodes) can be found online in the Supporting Information section at the end of this article. Supplementary figures show topographic surface AFM images, compositional analyses via EDS and XPS, and oxidation states of oxygen partial pressures dependent polycrystalline $CuBi_2O_4$ thin films in the Supplementary Figures 1, 2, and 3, respectively. Supplementary Table 1: a summary of reported stability and open-circuit voltages in the $CuBi_2O_4$ thin-film photocathodes. J. Woo et al., supplementary information of "Generation of Stable Photovoltage in Non-Stoichiometric $CuBi_2O_4$ Thin-Film Photocathodes," 2023. *(Supplementary Materials)*

References

[1] Y. Sun, J. Yang, S. Li, and D. Wang, "Defect engineering in perovskite oxide thin films," *Chemical Communications*, vol. 57, no. 68, pp. 8402–8420, 2021.

[2] S. Wang, W. Wei, T. Huang et al., "Nonstoichiometric oxygen-dependent microstructures and phase transitions in post-annealed vanadium dioxides," *Advanced Engineering Materials*, vol. 21, no. 7, p. 1801374, 2019.

[3] T. Raza, J. Yang, R. Wang et al., "Recent advance in physical description and material development for single component SOFC: a mini-review," *Chemical Engineering Journal*, vol. 444, article 136533, 2022.

[4] W. Banerjee, A. Kashir, and S. Kamba, "Hafnium oxide (HfO_2) – a multifunctional oxide: a review on the prospect and challenges of hafnium oxide in resistive switching and ferroelectric memories," *Small*, vol. 18, no. 23, article 2107575, 2022.

[5] V. Rajić, I. S. Simatović, L. Veselinović et al., "Bifunctional catalytic activity of $Zn_{1-x}Fe_xO$ toward the OER/ORR: seeking an optimal stoichiometry," *Physical Chemistry Chemical Physics*, vol. 22, no. 38, pp. 22078–22095, 2020.

[6] M. Radecka, A. Brudnik, K. Kulinowski et al., "Titanium dioxide thin films with controlled stoichiometry for photoelectrochemical systems," *Journal of Electronic Materials*, vol. 48, no. 9, pp. 5481–5490, 2019.

[7] J.-J. Velasco-Vélez, T. Jones, D. Gao et al., "The role of the copper oxidation state in the electrocatalytic reduction of CO_2 into valuable hydrocarbons," *ACS Sustainable Chemistry & Engineering*, vol. 7, no. 1, pp. 1485–1492, 2018.

[8] W. Yu, M. H. Richter, E. Simonoff, B. S. Brunschwig, and N. S. Lewis, "Investigations of the stability of GaAs for photoelectrochemical H_2 evolution in acidic or alkaline aqueous electrolytes," *Journal of Materials Chemistry A*, vol. 9, no. 40, pp. 22958–22972, 2021.

[9] D. Lee, W. Wang, C. Zhou et al., "The impact of surface composition on the interfacial energetics and photoelectrochemical properties of $BiVO_4$," *Nature Energy*, vol. 6, no. 3, pp. 287–294, 2021.

[10] D. K. Lee and K.-S. Choi, "Enhancing long-term photostability of $BiVO_4$ photoanodes for solar water splitting by tuning electrolyte composition," *Nature Energy*, vol. 3, no. 1, pp. 53–60, 2018.

[11] M. Kölbach, K. Harbauer, K. Ellmer, and R. van de Krol, "Elucidating the pulsed laser deposition process of $BiVO_4$ photoelectrodes for solar water splitting," *Journal of Physical Chemistry C*, vol. 124, no. 8, pp. 4438–4447, 2020.

[12] C. Li, J. He, Y. Xiao, Y. Li, and J.-J. Delaunay, "Earth-abundant Cu-based metal oxide photocathodes for photoelectrochemical water splitting," *Energy & Environmental Science*, vol. 13, no. 10, pp. 3269–3306, 2020.

[13] A. Paracchino, V. Laporte, K. Sivula, M. Grätzel, and E. Thimsen, "Highly active oxide photocathode for photoelectrochemical water reduction," *Nature Materials*, vol. 10, no. 6, pp. 456–461, 2011.

[14] I. Sullivan, B. Zoellner, and P. A. Maggard, "Copper(I)-based p-type oxides for photoelectrochemical and photovoltaic solar energy conversion," *Chemistry of Materials*, vol. 28, no. 17, pp. 5999–6016, 2016.

[15] S. P. Berglund, F. F. Abdi, P. Bogdanoff, A. Chemseddine, D. Friedrich, and R. van de Krol, "Comprehensive evaluation of CuBi2O4as a photocathode material for photoelectrochemical water splitting," *Chemistry of Materials*, vol. 28, no. 12, pp. 4231–4242, 2016.

[16] G. Sharma, Z. Zhao, P. Sarker et al., "Electronic structure, photovoltage, and photocatalytic hydrogen evolution with p-CuBi2O4 nanocrystals," *Journal of Materials Chemistry A*, vol. 4, no. 8, pp. 2936–2942, 2016.

[17] G. Seo, B. Kim, S. W. Hwang, S. S. Shin, and I. S. Cho, "High-performance bulky crystalline copper bismuthate photocathode for enhanced solar water splitting," *Nano Energy*, vol. 80, article 105568, 2021.

[18] J. Lee, H. Yoon, S. Kim et al., "Long-term stabilized high-density $CuBi_2O_4$/NiO heterostructure thin film photocathode grown by pulsed laser deposition," *Chemical Communications*, vol. 55, no. 83, pp. 12447–12450, 2019.

[19] J. Jin, J. Hu, J. Qu et al., "Reaction kinetics of photoelectrochemical CO2 reduction on a $CuBi_2O_4$-based photocathode," *ACS Applied Materials & Interfaces*, vol. 14, no. 15, pp. 17509–17519, 2022.

[20] S. A. Monny, L. Zhang, Z. Wang et al., "Fabricating highly efficient heterostructured CuBi2O4 photocathodes for unbiased water splitting," *Journal of Materials Chemistry A*, vol. 8, no. 5, pp. 2498–2504, 2020.

[21] J. Lee, H. Yoon, K. S. Choi et al., "Template engineering of $CuBi_2O_4$ single-crystal thin film photocathodes," *Small*, vol. 16, no. 39, p. 2002429, 2020.

[22] R. Gottesman, I. Levine, M. Schleuning et al., "Overcoming phase-purity challenges in complex metal oxide photoelectrodes: a case study of $CuBi_2O_4$," *Advanced Energy Materials*, vol. 11, no. 11, article 2003474, 2021.

[23] R. Gottesman, A. Song, I. Levine et al., "Pure CuBi2O4Photoelectrodes with increased stability by rapid thermal processing of Bi_2O_3/CuO grown by pulsed laser deposition," *Advanced Functional Materials*, vol. 30, no. 21, article 1910832, 2020.

[24] F. E. Oropeza, B. T. Feleki, K. H. Zhang, E. J. Hensen, and J. P. Hofmann, "Influence of reduced cu surface states on the photoelectrochemical properties of $CuBi_2O_4$," *ACS Applied Energy Materials*, vol. 2, no. 9, pp. 6866–6874, 2019.

[25] B. Tan, B. Liu, M. Sun, Y. Li, Z. Cao, and Z. Zhang, "Enhanced charge collection and surface activity of a CuBi2O4 photocathode via crystal facet engineering," *Journal of Materials Chemistry A*, vol. 10, no. 17, pp. 9427–9434, 2022.

[26] Z. Chen, H. N. Dinh, and E. Miller, *Photoelectrochemical Water Splitting, vol. 344*, Springer, 2013.

[27] J.-Y. Jung, J.-Y. Yu, and J.-H. Lee, "Dynamic photoelectrochemical device with open-circuit potential insensitive to thermodynamic voltage loss," *Journal of Physical Chemistry Letters*, vol. 9, no. 18, pp. 5412–5418, 2018.

[28] S. S. Kalanur, R. Singh, and H. Seo, "Enhanced solar water splitting of an ideally doped and work function tuned {002} oriented one-dimensional WO_3 with nanoscale surface charge mapping insights," *Applied Catalysis B: Environmental*, vol. 295, article 120269, 2021.

[29] Y. Wang, H. Wang, A. R. Woldu, X. Zhang, and T. He, "Optimization of charge behavior in nanoporous $CuBi_2O_4$ photocathode for photoelectrochemical reduction of CO_2," *Catalysis Today*, vol. 335, pp. 388–394, 2019.

[30] S.-M. Park, T. Ikegami, and K. Ebihara, "Effects of substrate temperature on the properties of Ga-doped ZnO by pulsed laser deposition," *Thin Solid Films*, vol. 513, no. 1–2, pp. 90–94, 2006.

[31] T. K. O. Vu, D. U. Lee, and E. K. Kim, "The effect of oxygen partial pressure on band gap modulation of Ga_2O_3 grown by pulsed laser deposition," *Journal of Alloys and Compounds*, vol. 806, pp. 874–880, 2019.

[32] E. Breckenfeld, Z. Chen, A. R. Damodaran, and L. W. Martin, "Effects of nonequilibrium growth, nonstoichiometry, and film orientation on the metal-to-insulator transition in $NdNiO_3$ thin films," *ACS Applied Materials & Interfaces*, vol. 6, no. 24, pp. 22436–22444, 2014.

[33] J. Chen, M. Döbeli, D. Stender et al., "Tracing the origin of oxygen for $La_{0.6}Sr_{0.4}MnO_3$ thin film growth by pulsed laser deposition," *Journal of Physics D: Applied Physics*, vol. 49, no. 4, article 045201, 2015.

[34] E. Enriquez, A. Chen, Z. Harrell et al., "Oxygen vacancy-tuned physical properties in perovskite thin films with multiple B-site valance states," *Scientific Reports*, vol. 7, no. 1, pp. 1–8, 2017.

[35] F. X. Zhang and S. K. Saxena, "Raman studies of Bi_2CuO_4 at high pressures," *Applied Physics Letters*, vol. 88, no. 14, article 141926, 2006.

[36] R. Patil, S. Kelkar, R. Naphade, and S. Ogale, "Low temperature grown $CuBi_2O_4$ with flower morphology and its composite with CuO nanosheets for photoelectrochemical water splitting," *Journal of Materials Chemistry A*, vol. 2, no. 10, pp. 3661–3668, 2014.

[37] N. Nurmalasari, Y. Yulizar, and D. O. B. Apriandanu, "Bi2O3-nanoparticles: synthesis, characterizations, and photocatalytic activity," *IOP Conference Series: Materials Science and Engineering*, vol. 763, no. 1, article 012036, 2020.

[38] V. Dolocan and F. Iova, "Optical properties of Bi_2O_3 thin films," *Physica Status Solidi A: Applications and Materials Science*, vol. 64, no. 2, pp. 755–759, 1981.

[39] Z. Zhang, S. A. Lindley, R. Dhall et al., "Beneficial CuO phase segregation in the ternary p-type oxide photocathode $CuBi_2O_4$," *ACS Applied Energy Materials*, vol. 2, no. 6, pp. 4111–4117, 2019.